Oxidation modes and thermodynamics of Fe^{II-III} oxyhydroxycarbonate green rust: dissolution-precipitation versus *in-situ* deprotonation; about the fougerite mineral

Christian Ruby[a], Mustapha Abdelmoula[a], Sébastien Naille[a], Aurélien Renard[a], Varsha Khare[a], Georges Ona-Nguema[b], Guillaume Morin[b], Jean-Marie R. Génin[c]

[a] *Institut Jean Barriol, FR 2843, Laboratoire de Chimie Physique et Microbiologie pour l'Environnement, LCPME UMR7564 UHP-CNRS, Nancy Université, 405 rue de Vandoeuvre, 54600 Villers-lès-Nancy, France*

[b] *Institut de Minéralogie et de Physique des Milieux Condensés (IMPMC), Université Paris 6 et Paris 7; IPGP; CNRS; 140, rue de Lourmel, 75015 Paris, France*

[c] *Institut Jean Barriol, FR 2843 CNRS-Université Henri Poincaré, Nancy Université, Service des Matériaux pour le Développement Durable, l'Energie et l'Environnement, Ecole Supérieure des Sciences et Technologies de l'Ingénieur de Nancy 2 rue Jean Lamour, 54500 Vandoeuvre-lès-Nancy, France*

Corresponding author:

Christian Ruby,

IJB-LCPME, 405, rue de Vandoeuvre, 54600 Villers-lès-Nancy, France.

Tel: 33 3 83 68 52 20

Fax: 33 3 83 27 54 44

E-mail: Christian.ruby@lcpme.cnrs-nancy.fr

Submitted to *Geochim. Cosmochim. Acta*
June 2009

Keywords: Fe^{II-III} oxyhydroxycarbonate, carbonated green rust, fougerite, gleysol, Mössbauer spectroscopy, XRD

Abstract

Fe^{II-III} hydroxycarbonate green rust $GR(CO_3^{2-})$, $Fe^{II}_4\ Fe^{III}_2\ (OH)_{12}\ CO_3 \bullet 3H_2O$, is oxidized in aqueous solutions with varying reaction kinetics. Rapid oxidation with either H_2O_2 or dissolved oxygen under neutral and alkaline conditions leads to the formation of ferric oxyhydroxycarbonate $GR(CO_3^{2-})^*$, $Fe^{III}_6\ O_{12}\ H_8\ CO_3 \bullet 3H_2O$, via a solid-state reaction. By decreasing the flow of oxygen bubbled in the solution, goethite α-FeOOH forms by dissolution-precipitation mechanism whereas a mixture of non-stoichiometric magnetite $Fe_{(3-x)}O_4$ and goethite is observed for lower oxidation rates. The intermediate Fe^{II-III} oxyhydroxycarbonate of formula $Fe^{II}_{6(1-x)}\ Fe^{III}_{6x}\ O_{12}\ H_{2(7-3x)}\ CO_3 \bullet 3H_2O$, i.e. $GR(x)^*$ for which $x \in [1/3, 1]$, is the synthetic compound that is homologous to the fougerite mineral present in hydromorphic gleysol; *in situ* oxidation accounts for the variation of ferric molar fraction $x = [Fe^{III}]/\{[Fe^{II}]+[Fe^{III}]\}$ observed in the field as a function of depth and season but limited to the range [1/3, 2/3]. The domain of stability for partially oxidized green rust is observed in the E_h-pH Pourbaix diagrams if thermodynamic properties of $GR(x)^*$ is compared with those of lepidocrocite, γ-FeOOH, and goethite, α-FeOOH. Electrochemical equilibrium between $GR(x)^*$ and Fe^{II} in solution corresponds to E_h-pH conditions close to those measured in the field. Therefore, the reductive dissolution of $GR(x)^*$ can explain the relatively large concentration of Fe^{II} measured in aqueous medium of hydromorphic soils containing fougerite.

1. INTRODUCTION

Hydromorphic soil colour has been described long ago defining a so-called gleysol (Vysostskii, 1905). A typical example of the profile with depth presents (i) some few cm thick organic top cover that comprises humic substances, (ii) an upper mineral layer that can reach two meters deep getting ochre progressively with scattered orange dots, and (iii) the gley under the water-table, which resembles celadon porcelain of pale bluish-green colour and looks homogeneous and ductile. The change from ochre to bluish-green was attributed long ago to a change of iron state from ferric to ferrous, creating a redox front following the water level (Vysostskii, 1905; Taylor, 1980, 1982; Ernstsen and Mørup, 1992; Ernstsen, 1996). However, the mineral that incorporates Fe^{II} cations remained a mystery till ^{57}Fe Mössbauer spectra showed in 1996 that it was in fact a Fe^{II-III} green rust (GR) compound as encountered during the corrosion process of iron-base materials (Trolard et al., 1997; Génin et al., 1998b). It was christened fougerite (IMA 2003-057) since the first extracted samples came from the State-owned forest of Fougères (Brittany-France). Unfortunately, even though the Mössbauer spectra displayed hyperfine parameters such as isomer shifts δ and quadrupole splittings Δ that were definitively those of a green rust (Murad and Taylor, 1984; Génin et al., 1986; Olowe et al. 1987; Drissi et al., 1994; Génin et al., 1998a), component intensities did not match those observed for green rusts prepared in the laboratory and X ray diffraction (XRD) was of no use at that time since the fougerite mineral is in minority and cannot diffract with enough intensity to be distinguished from a mixture of patterns of many other mineral compounds (Génin et al., 1998b). In contrast, ^{57}Co γ-ray resonance, which is only sensitive to iron-containing minerals, was appropriate for revealing that it was a green rust but without designating which type.

Since the early works of Girard and Chaudron (1935), Feitknecht and Keller (1950) or Bernal et al. (1959), Fe^{II-III} hydroxysalt GR compounds were known to be intermediate products that occur during the oxidation of Fe^{II} species into Fe^{III} containing solid compounds, i.e. the ferric oxyhydroxides such as goethite α-FeOOH, lepidocrocite γ-FeOOH or ferrihydrite. They belong to the layered double hydroxide (LDH) family and obey to the general formula $[M^{II}_{(1-x)} M^{III}_{x} (OH)_2]^{x+} \bullet [(x/n) A^{n-} (m/n) H_2O]^{x-}$ where M^{II} and M^{III} are di- and trivalent metallic cations incorporated within positively charged brucite-type layers where each cation lies at the centre of an octahedron with OH^- ions at its six apices, and A^{n-} are anions situated in interlayers whereas $x = [M^{III}]/\{[M^{II}]+[M^{III}]\}$ represents the trivalent cation molar fraction, the value of which lies between 0.25 and 0.33 (Hansen, 2001; Génin et al., 2006a; Ruby et al., 2006b).

The oxidation of GR in the air is a naturally occurring process, the study of which was initiated by Feitknecht and Keller (1950) and Bernal et al. (1959). They carried out oxidation experiments of Fe^{II} aqueous suspension containing different anions, e.g. SO_4^{2-} and Cl^-, in order to obtain a better understanding of the various transformations that occur during the corrosion of iron. More recently, systematic studies involving many anions displayed kinetics comprising three stages as observed from the plateaus recorded in the electrode potential E_h or pH versus time curves monitored during the oxidation process of the initial ferrous hydroxide precipitate $Fe(OH)_2$. In particular, chloride, sulphate and carbonate-containing media were followed for drawing E_h-pH Pourbaix diagrams of the afferent GR, respectively (Refait et al., 1993; Génin et al., 1996; Drissi et al., 1995; Génin et al., 2006b). The usual domain of corrosion of iron-base materials and steels was consequently correlated to the domain of existence of the intermediate GR that forms at their surface and which dissolves during the further oxidation and precipitates into ferric oxyhydroxides; this is the most common dissolution-precipitation process.

X-ray absorption studies definitively confirmed that the arrangement of Fe cations in the basal (0001) planes of the fougerite mineral is similar to that observed in synthetic Fe^{II-III} hydroxycarbonate green rust compound, GR(CO_3^{2-}), and in Mg^{II}-Fe^{III} hydroxycarbonate homologous to the pyroaurite mineral (Refait et al., 2001). The possible presence of carbonate anions inside GR-type soil samples was initially suggested by Taylor et al. (1980). Indeed, carbonate species may easily be present in the interlayers owing to their very strong affinity for the LDH structure if compared to other anions (Hansen, 2001) and to their ubiquity in nature. Nevertheless, direct spectroscopic evidence concerning the exact nature of the anion inserted within fougerite from a natural sample was still lacking.

Discrepancies between mineral samples and green rusts as prepared in the laboratory in the late 90's were attributed to their mode of formation; the first ones were assumed to be due to bacterial reduction of ferric minerals in anoxic conditions under the water table whereas the second ones were prepared cautiously by oxidation of $Fe(OH)_2$. This explanation was definitively confirmed when Ona-Nguena et al. (2002) demonstrated that a carbonated green rust could be produced in anoxic conditions by reducing some lepidocrocite γ-FeOOH in the presence of dissimilatory iron-reducing bacteria, *Shewanella putrefaciens*. Moreover, the ferric molar ratio *x* was larger than 1/3 as observed in the mineral samples.

Bernal et al. (1959) found also that a rapid oxidation by H_2O_2 of ferrous hydroxide $Fe(OH)_2$ led to a ferric compound homologous to a natural mineral known as ferroxyhite δ'-FeOOH. Taylor (1980) and Hansen (1989) observed the same kind of phenomenon when a Fe^{II-III} hydroxycarbonate, GR(CO_3^{2-}), previously formed in aqueous solution, was filtered and exposed to the air. Few years later, during the aerial oxidation of a dry hydroxycarbonate GR(CO_3^{2-}) that appeared on the top of an α-Fe foil, Abdelmoula et al. (1996) observed the formation of goethite mixed with another ferric compound characterized by an interplanar distance d = 7.34 Å that was thus assumed to keep the layer sequence found in GR(CO_3^{2-}).

Refait et al. (2003) proceeded similarly to study the fast oxidation by H_2O_2 of Fe^{II-III} hydroxychloride GR(Cl^-) in aqueous medium and noted that a ferric product of oxidation identified by Mössbauer spectroscopy had XRD lines practically at the same positions as those observed for GR(Cl^-); that compound was thus called "ferric green rust, GR(Cl^-)*". The same property was observed with hydroxycarbonate GR(CO_3^{2-}) when Legrand et al. (2001) showed that it could also get oxidized into a ferric compound that was called "ex-GR" by voltammetric cycling and later with dissolved oxygen by avoiding the dissolution-precipitation process (Legrand et al., 2004).

More recently, GR(CO_3^{2-}) got oxidized progressively into the "ferric green rust", by means of Fe^{II-III} oxyhydroxycarbonate GR(x)* characterised by a ferric molar ratio $x = [Fe^{III}]/[Fe_{total}]$ that varies continuously from 1/3 to 1 (Génin et al., 2006a; Ruby et al., 2006a). A progressive deprotonation of the hydroxyl sheets within the layered structure was proposed to explain the process along with a slight structural change (Génin et al., 2006c) and this assumption was definitively validated using X-Ray photoelectron spectroscopy (Mullet et al., 2008). Therefore, the fully oxidized "ferric green rust" with x =1, i.e. $Fe^{III}_6 O_{12} H_8 CO_3 \bullet 3H_2O$ is the ferric oxyhydroxycarbonate GR(CO_3^{2-})* and the intermediate Fe^{II-III} oxyhydroxycarbonate, $Fe^{II}_{6(1-x)} Fe^{III}_{6x} O_{12} H_{2(7-3x)} CO_3 \bullet 3H_2O$, GR($x$)* for which $x \in [1/3, 1]$ that gets oxidized *in situ*, represents some new kind of solid phase that resembles another well known example such as magnetite Fe_3O_4 that can also get oxidized *in situ* into maghemite γ-Fe_2O_3. Finally, the structure of ferric oxyhydroxycarbonate GR(CO_3^{2-})* (Génin et al., 2005, 2006c) and the comparison between its ferromagnetic behaviour with a Curie point around 70 K whereas Fe^{II-III} hydroxycarbonate GR(CO_3^{2-}) is ferrimagnetic with a Néel temperature at 5 K (Rusch et al., 2008) have been discussed displaying a long range ordering among Fe^{II} and Fe^{III} cations.

The main goal of this paper is to determine the kinetics threshold that controls the transformation of GR(CO_3^{2-}), either into ferric oxyhydroxycarbonate GR(CO_3^{2-})* by *in situ*

deprotonation, or into ferric oxyhydroxide FeOOH such as goethite by dissolution-precipitation process. Either the addition of a controlled amount of a strong oxidant (H_2O_2) or various oxygen flow rates were used for this purpose. It will provide a useful characterisation of the GR(*x*)* compounds for the full range of *x* values that scan from 1/3 to 1 obtained by using X-ray diffraction (XRD) and γ-ray backscattered Mössbauer spectroscopy at room temperature. The same apparatus used recently for field experiments when studying *in situ* the mineralogical transformations of fougerite (Féder et al., 2005; Rodionov et al., 2006), i.e. the miniaturised Mössbauer spectrometer (MIMOSII) developed by Klingelhöfer et al. (1996) was used here for the characterization of synthetic GR compounds. These studies confirmed the redox flexibility of the fougerite mineral with depth, time and weather conditions in the water table through the variability of the ferric molar ratio *x* that fluctuates in the [0.33-0.67] range. Finally, a definitive identification of green rust in groundwater has been very recently done in Denmark (Christiansen et al., 2009) and for the first time XRD patterns of the mineral are displayed; these patterns demonstrate that the distance between layers, ~ 7.6 Å, is that of the GR where carbonate anions are inserted.

Consequently, since the identification of the exact nature of the green rust mineral in ground water is now completely established with no ambiguity, time happens to know more about the properties of its chemical counterpart, the Fe^{II-III} oxyhydroxycarbonate GR(*x*)* that is limited to the range [0.33-0.67], in particular its thermodynamics; let us demonstrate that field data found in the literature are indeed consistent with measurements made from synthetic samples within the same range [0.33-0.67]. In this paper, the thermodynamic properties of GR(*x*)* are compared to those of lepidocrocite γ-FeOOH and goethite α-FeOOH by obtaining their domains of stability in various E_h-pH Pourbaix diagrams. Results are discussed at the light of the two possible modes of oxidation, i.e. by dissolution-precipitation or by *in situ*

deprotonation within the solid state, showing that the second mode should occur in natural conditions.

2. EXPERIMENTAL

2.1. Synthesis of initial Fe^{II-III} hydroxycarbonate

An initial GR(CO_3^{2-}) precipitate was prepared in a 1 L and 20 cm diameter gas tight reactor, which a continuous flux of bubbled nitrogen passed through, at a controlled temperature of 20°C. Electrode potential E_h (V) and pH were measured continuously. An Ag/AgCl electrode (3 M KCl) was used for measuring E_h, but values were reported with respect to the standard hydrogen electrode, i.e. $E_h(V) = E_{Ag/AgCl}(V) + 0.211$ V. A 600 mL salt mixture of $Fe(SO_4) \cdot 7H_2O$ and $Fe_2(SO_4)_3 \cdot 5H_2O$ was progressively neutralised with 37 mL of Na_2CO_3 solution ($[Fe^{II}] = 2.2\times10^{-2}$ M, $[Fe^{III}] = 1.1\times10^{-2}$ M, $[Na_2CO_3] = 1.1$ M) (Bocher et al., 2004; Aïssa et al., 2006). The suspension got homogenous by stirring with a magnetic rod under a continuous flux of nitrogen bubbling. The pH was about 9.3 once the basic solution was added.

2.2. Violent oxidation of Fe^{II-III} hydroxycarbonate by hydrogen peroxide H_2O_2

These experiments were devised to ensure the *in situ* oxidation of GR(CO_3^{2-}) within the solid state of a given amount of Fe^{II} species. Therefore, adequate amounts of H_2O_2 were added into the initial GR(CO_3^{2-}) suspension to oxidise to increasing values of ferric molar fraction *x*, i.e. 0.5, 0.67, 0.83 and 1 as previously described (Ruby et al., 2006a). A small amount of $Na_2HPO_4 \cdot 12 H_2O$ salt was dissolved in the suspension ($[PO_4] = 4\times10^{-4}$ M) before adding H_2O_2. The rapidity of oxidation due to the use of a strong oxidant and the presence of phosphate anions both hindered CO_3^{2-} anions to escape from the GR structure and favoured

consequently the formation of GR(*x*)* by *in situ* solid-state oxidation as previously discussed (Legrand et al., 2004; Génin et al., 2006c). These samples were used to get XRD patterns and backscattered Mössbauer spectra recorded at room temperature for reference.

2.3. Slow oxidation of Fe^{II-III} hydroxycarbonate by O_2 bubbling

No phosphate anions were added initially in the GR(CO_3^{2-}) suspension in contrast to the H_2O_2 oxidation experiments. A mixture of synthetic air (21 % O_2, 79 % N_2) and nitrogen (100% N_2) was bubbled into the solution at a constant flow rate of ~ 2.5×10^{-3} L s^{-1}. The ratio between the partial pressure of oxygen and the total gas pressure $X(O_2) = [p(O_2) / p_{total}]$ was maintained at 2.7, 6.7, 13.3 and 21 %. The oxygen gas flow $F(O_2)$ varied between 0.4 and 2.9 moles of O_2 per day (Table 1). The stirring by the magnetic rod was maintained at 375 rpm and the initial pH of 9.3 remained constant all along the oxidation process.

2.4. Fast oxidation of Fe^{II-III} hydroxycarbonate in the air

N_2 bubbling was stopped and the reactor was exposed to the air. A vigorous magnetic stirring was set at 750 rpm in order to accelerate the oxidation process. The final pH observed at the end of the co-precipitation experiments decreased slightly from 9.3 to 9. In a second experiment, the final pH obtained at the end of the GR(CO_3^{2-}) co-precipitation, i.e. pH = 9.3, was adjusted with a concentrated HCl solution at a value of 7 ± 0.2. The same air oxidation experiment was performed by maintaining a constant pH of 7.

2.5. Characterization of solids

2.5.1. X-ray diffraction (XRD)

The partially oxidized samples of the experiments performed with H_2O_2 (section 2.2) were filtered and dried in a glove box filled with nitrogen during about one day. The dried powder was thoroughly crushed, mixed with a small quantity of NaCl used as an internal reference and introduced into a 0.5 mm glass capillary. The tube was closed with some glue under nitrogen in a glove box to avoid further air oxidation. XRD patterns were recorded with a Panalytical X'Pert Pro MPD® diffractometer mounted in the Debye-Scherrer configuration, using an elliptical mirror to obtain a high flux, parallel incident beam and an X'Celerator® detector to collect diffracted beams. Data were recorded with monochromatic CoK_α beam (λ = 0.17889 nm) in continuous scan mode within a (5-75°) 2θ range with steps of 0.0167°. The fully oxidized sample of the O_2 bubbling and air oxidation experiments (section 2.3 & 2.4) were filtered and air dried. Samples were introduced in 1 mm diameter glass capillaries and X-ray diffractograms were recorded with a goniometer equipped with an INEL 120 PSD® counter coupled to a Rigaku® 12 kW rotating anode with MoK_α source (λ = 0.07093 nm).

2.5.2. Mössbauer spectroscopy

Partially oxidized samples were filtered in a glove box filled with an inert N_2 atmosphere. The filtered samples were inserted into a ~ 3 cm^2 holder and were set into a gas tight cell specially designed to perform Mössbauer reflexion analyses at room temperature under a continuous inert N_2 gas flow. No significant variation of the molar ratio $x = Fe^{III} / (Fe^{II}+Fe^{III})$ ratio was observed during the whole analysis time (~ 48 hours). Reemitted backscattered γ-rays (14.4 keV) were selected by four Si-PIN-diodes detectors. Center shifts *CS* were reported with respect to that of α-Fe at room temperature. Mössbauer

spectra were computer-fitted with either a sum of Lorentzian shape lines (x = 0.33) or a Voigt profile analyses (x = 0.5, 0.67, 0.83 and 1).

3. RESULTS

3.1. Oxidation of Fe^{II-III} hydroxycarbonate GR(CO_3^{2-}) with hydrogen peroxide H_2O_2

*3.1.1. XRD patterns of Fe^{II-III} oxyhydroxycarbonate GR(*x*)**

The evolution of the XRD patterns for increasing values of ferric molar fraction x is presented in Fig. 1 by using the same scale for all patterns. Diffractogram of GR(CO_3^{2-}) i.e. $Fe^{II}_4\ Fe^{III}_2\ (OH)_{12}\ CO_3 \bullet 3H_2O$ at stoichiometry, is characterized by an exceptional sharpness of lines, (Fig. 1aα) that were already observed in previous studies (Taylor et al., 1980; Drissi et al., 1995; Aïssa et al., 2006). This series of peaks are also clearly visible for x values of 0.5 and 0.67 showing that the GR(CO_3^{2-}) original stacking sequence of cation layers and anion interlayers is maintained within the structure [Fig. 1a(β & γ)]. A degradation of the diffractogram is observed with global peak broadening when x increases and some lines are no longer detectable for x values of 0.83 and 1 [Fig. 1a(δ & ε)]. Nevertheless, the main line of the initial GR(CO_3^{2-}) pattern, i.e. the (003) line, is observed for all samples even though its intensity decreases significantly along with its broadening for the highest values of x as shown into more details (Fig. 1b). The most interesting feature is the continuous shift of this peak towards higher angles when x increases. Values of interplanar distances d_{003} along the ***c*** axis are estimated (Table 2). A continuous contraction of the d_{003} distance is thus measured and a maximal relative variation of ~ 4% is computed for the fully oxidized sample (x = 1). For x values situated between 0.33 and 0.67, since the initial GR(CO_3^{2-}) structure is maintained, a first estimation of the ***a*** and ***c*** cell parameters is computed by using respectively the (001) and

(102) diffraction lines (Table 2). For this range of *x* values, a very small contraction of ***a*** and ***c*** parameters is measured with a relative variation comprised between about 0.5 and 1%.

3.1.2. Backscattered Mössbauer spectra of Fe^{II-III} oxyhydroxycarbonate

Backscattered Mössbauer spectra recorded at 300 K of GR(CO_3^{2-}) and GR(*x*)* where *x* scan the domain]0.33-1] are presented in Fig. 2. The spectrum of hydroxycarbonate green rust GR(CO_3^{2-}) for $x = 0.33$ [Fig. 2(α)] is adjusted with one ferric doublet (D_3) and two ferrous doublets (D_1 and D_2) as usual (Génin et al. 2006a). The hyperfine parameters are reported in Table 3. As previously observed by using transmission Mössbauer spectroscopy at 78 K (Génin et al., 2006c), the violent oxidation leads to both the expected decrease of the Fe^{II} components and the global broadening of the spectra [Fig. 2(β-ε)]. Therefore, Voigt profile analysis is used for curve fitting of oxidised samples. Note that this behaviour is concomitant to the broadening observed by XRD [Fig. 1(α-ε)]. The validity of the models is provided by the good agreement between the targeted values of *x* and those measured with Mössbauer spectroscopy (cf. the two last columns of Table 3). The fully oxidized sample ($x = 1$) is fitted with a broad Fe^{III} paramagnetic doublet *D*.

3.2. Oxidation of Fe^{II-III} hydroxycarbonate GR(CO_3^{2-}) in the air

3.2.1. Slow oxidation by controlled {O_2 + N_2} bubbling

Fe^{II-III} hydroxycarbonate GR(CO_3^{2-}) was oxidized with varying relative oxygen concentrations $X(O_2)$ modulated by the gas flow with a rotation of 375 rpm for the magnetic rod. The pH did not vary significantly during the experiment and was measured to be close to 9 as due to the buffering effect of the carbonate species. The evolution of the redox potential E_h as a function of oxidation time corresponding to different oxygen contents $X(O_2)$ into the bubbling gas is presented in Fig. 3a. Curves α, β & γ are characterised by two plateaus

separated by an equivalent point E. Around point E, the initial dark-blue colour of the suspension becomes rapidly yellow-brown. Point E is attributed to the end of oxidation and its abscissa t_f shifts towards longer periods when $X(O_2)$ decreases. Curve δ exhibits two plateaus separated by point P before reaching point E for the lowest oxygen concentration $X(O_2)$ at 2.7%. Note also that a hook H is distinguished on all curves (Fig. 3a) at the beginning of the oxidation process and that its height increases with $X(O_2)$.

A mean oxidation velocity defined as $V(O_2) = [n(O_2) / t_f]$ is evaluated in Table 1 where $n(O_2)$ is the number of oxygen moles that are consumed and corresponds to the Fe^{II} species present in the initial $GR(CO_3^{2-})$ compound. The oxidation efficiency is calculated from the ratio $[V(O_2) / F(O_2)]$ and stays practically constant, situated at a relatively low value of about 1%. XRD shows that goethite forms for $X(O_2)$ values of 20, 13.3 and 6.7% (Fig. 4b), whereas the oxidation leads to a mixture of magnetite and goethite for the lowest oxygen concentration $X(O_2)$ = 2.7% (Fig. 4a). Mössbauer spectrum measured at room temperature confirms that non-stoechiometric magnetite forms (Vandenberghe et al., 2000) and that only 12% of the Fe atoms are present into α-FeOOH (Fig. 5a, Table 4). According to the corresponding XRD results, doublet *D* in the central part of the spectrum (Fig. 5a) must be attributed to Fe^{III} species present in superparamagnetic crystals of low size (< ~100 nm); this explains the spectral behaviour of α-FeOOH governed by relaxation at room temperature. A similar behaviour is observed for goethite that forms alone at higher oxygen concentrations (Fig. 5b) where doublet *D* becomes a magnetic sextet as due to an increase of crystal size.

3.2.2. Fast oxidation of $GR(CO_3^{2-})$ in the air

The evolution of redox potential E_h for pH values of 9 and 7 is presented in Fig. 3b with fast oxidation using now a rotation of 750 rpm for the magnetic rod. The trend is significantly different if compared to the previous $\{O_2 + N_2\}$ bubbling experiments (Fig. 3a): (i) a gradual

increase of E_h is observed along with the absence of defined equivalent points, (ii) the kinetics of oxidation is much faster (the time scale is enlarged) and the final E_h plateau situated between +300 and +400 mV is reached between 2 and 8 times more rapidly. In contrast, the pH does not seem to influence the kinetics of the reaction since a constant value of redox potential is reached after ~ 80 minutes in both experiments (pH = 7 and 9). XRD patterns (Fig. 4c) show that the end product of oxidation in both cases is now the ferric oxyhydroxycarbonate GR(CO_3^{2-})* that is characterized by two main lines in good agreement with literature (Legrand et al., 2004; Génin et al., 2006c). Similarly, a paramagnetic doublet is observed for this sample in the Mössbauer spectrum recorded at room temperature for both experiments performed either at pH = 9 or 7 (Fig. 5c).

4. DISCUSSION

4.1. Air oxidation of Fe^{II-III} hydroxycarbonate GR(CO_3^{2-})

The oxidation of GR(CO_3^{2-}) by dissolved O_2 carbonated aqueous medium was the subject of previous studies (Drissi et al., 1995; Benali et al., 2001; Legrand et al., 2004; Refait et al., 2007) that led to some kind of a controversy about the exact nature of final products. Benali et al. (2001) as well as Refait et al. (2007) observed that the main final oxidation product was goethite α-FeOOH at a pH between around 8 and 9 of the aqueous solution. According to Benali et al. (2001), the formation of goethite was preceded by the precipitation of a less crystallised compound known as ferrihydrite. In contrast, Legrand et al (2004) who studied the same reaction under experimental conditions that looked similar at a first glance, observed the formation of a ferric compound that was the ferric oxyhydroxycarbonate GR(CO_3^{2-})* or a mixture of GR(CO_3^{2-})* with some lepidocrocite γ-FeOOH. A slow transformation of ferric

$GR(CO_3^{2-})$* into goethite was proposed to occur only after aging in the suspension. Here, our study clearly shows that either goethite or $GR(CO_3^{2-})$* can form as final product of oxidation by changing merely the oxygen flow rate introduced into the $GR(CO_3^{2-})$ aqueous suspension: (i) if $GR(CO_3^{2-})$ gets oxidized into goethite, a plateau of redox potential E_h followed by a well defined equivalent point at the end of the oxidation process is observed (Fig. 3) (see also Benali et al., 2001; Refait et al., 2007); (ii) if $GR(CO_3^{2-})$ gets oxidized *in situ* into ferric $GR(CO_3^{2-})$*, a continuous increase of redox potential is obtained that reaches its maximum when all Fe^{II} species are converted into Fe^{III} species. This last process is much faster than that by dissolution-precipitation as testified by the change of time scale (Fig. 3a versus 3b). The redox potential plateau corresponds to an electrochemical equilibrium between two solid compounds that have different structures, here $GR(CO_3^{2-})$ and α-FeOOH, whereas the progressive increase of E_h must be attributed to an *in situ* oxidation of $GR(CO_3^{2-})$ that occurs within one unique solid compound (Fig. 3a) . In contrast, the behaviour of the redox potential (Fig. 3b) is similar to that obtained when $GR(CO_3^{2-})$ got oxidized *in situ* up to $GR(CO_3^{2-})$* by progressive addition of H_2O_2 (Génin et al., 2006c; Ruby et al., 2006a). In both cases, values of E_h can be estimated by Nernst's law if equilibrium is assumed. Therefore, the evolution of the redox potential can be used as a guide for determining which oxidation path is followed by $GR(CO_3^{2-})$, i.e. either by dissolution-precipitation or by *in situ* deprotonation within the solid state. The observation of the experimental results quoted previously, i.e. Fig. 1a (Benali et al., 2001) and Fig. 1 (Legrand et al., 2004), demonstrate clearly that the oxidation paths were in fact different in both experiments and consequently led to different final oxidation products. According to our results (Fig. 3a), the aeration conditions of aqueous solution explain fully the difference. Finally the hook H observed at the beginning of the dissolution-precipitation process (Fig. 3a) was in fact due to a short period of *in situ* deprotonation that was not maintained.

4.2. Oxidation of Fe^{II-III} (oxy)hydroxycarbonate and fougerite

The evolution of XRD patterns confirms the progressive contraction of the structure previously presented for a partially oxidized GR* at x = 0.5 and fully ferric one (Fig. 1) (Génin et al., 2006c; Ruby et al., 2006a). Broadening of peaks observed for ferric GR(CO_3^{2-})* was then attributed to a significant local distortion whereas the overall hexagonal morphology of the crystal as observed by TEM was conserved. A lattice contraction is in good agreement with the proposed deprotonation of the hydroxyl ions in octahedral coordination with iron, which was recently confirmed by X-ray photoelectron spectroscopy (Mullet et al., 2008). In general, the density of Fe-containing compounds increases from hydroxide to oxyhydroxide and finally to oxide. Such mineralogical transformation may also occur in hydromorphic soils where fougerite, i.e. the homologous mineral of GR(x)*, was identified (Trolard et al., 1997; Génin et al., 1998b). However, the x values observed in fougerite varied between 1/3 and 2/3 depending on the depth and weather conditions by using MIMOS spectrometer where fast and reversible mineralogical transformations of iron oxides exist in these soils (Féder et al., 2005). Because laboratory observations demonstrate here that fast kinetics experiments lead to an *in situ* transformation of GR(x)* within the solid, such processes may also easily occur in hydromorphic soils. Obviously, the deprotonation effect that occurs *in situ* during the oxidation of GR(x)* is much more rapid and flexible than the dissolution-precipitation mechanism.

4.2.1. Dissolution-precipitation oxidation mechanism

The mechanism of oxidation of $Fe(OH)_2$ in carbonated media was developed by Drissi et al. (1994, 1995) according to two stages that follow the evolution of E_h with time (Génin et al., 2006b):

A first stage corresponds to the precipitation of GR(CO_3^{2-}) according to:

$$5\ Fe^{II}(OH)_2 + Fe^{II}_{aq} + CO_3^{2-} + 1/2\ O_2 + H_2O \Leftrightarrow Fe^{II}_4\,Fe^{III}_2\,(OH)_{12}\,CO_3 \quad (1)$$

A second stage corresponds to the dissolution of GR(CO_3^{2-}) followed by precipitation of a ferric oxyhydroxide $Fe^{III}OOH$:

$$Fe^{II}_4\,Fe^{III}_2\,(OH)_{12}\,CO_3 + 3/4\ O_2 \Leftrightarrow 5\ Fe^{III}OOH + Fe^{II}_{aq} + CO_3^{2-} + 7/2\ H_2O \quad (2)$$

According to Benali et al. (2001), the most disorganised ferric oxyhydroxide, i.e. ferrihydrite, forms in most common experimental conditions. Carbonate anions are back into solution and part of Fe^{II} ions does not get oxidized. It is followed by the formation of goethite, the most stable ferric oxyhydroxide, according to reaction (3), which can last forever and may even stop before its completion:

$$5\ Fe^{III}OOH + Fe^{II}_{aq} + 1/4\ O_2 + 2\ OH^- \Leftrightarrow 6\ \alpha\text{-}Fe^{III}OOH + 1/2\ H_2O \quad (3)$$

At lower oxygen concentrations, reaction (2) may be replaced by the following:

$$Fe^{II}_4\,Fe^{III}_2\,(OH)_{12}\,CO_3 + 1/3\ O_2 \Leftrightarrow 5/3\ Fe^{II}\,Fe^{III}_2\,O_4 + Fe^{II}_{aq} + CO_3^{2-} + 6\ H_2O \quad (4)$$

Again, carbonate anions are back into solution and part of Fe^{II} ions is not yet oxidized and remains in solution. If both reactions (2) and (4) are active, a mixture of FeOOH and Fe_3O_4 can be obtained as observed by XRD and Mössbauer spectroscopy (Fig. 4a & 5a). The two separated plateaus (Fig. 3) on both sides of point P are due to a change of reaction: (i) reaction (4) that leads to magnetite occurs at a lower redox potential, i.e. at E_h values on the right side of point P and, (ii) reaction (2) occurs at higher E_h values on the left side. This proves that Fe_3O_4, which has a lower potential than FeOOH since it still comprises some Fe^{II} ions, appears afterwards in regions of the solution where oxygen is harder to diffuse. Reactions (1), (2), (3) and (4) are illustrated in the Fe^{II}-Fe^{III} mass-balance diagram (Ruby et al., 2006b, 2006c) (Fig. 6a). Reaction (1), which is common for the two processes, corresponds to the precipitation of GR(CO_3^{2-}) and is represented by segment AB. Reactions (2) and (4) correspond to the segments that link point B to D and B to C, respectively. Points C and D lie

on the tie-lines IF and IE. Thus, they represent mixtures of Fe^{II}_{aq} (point I) and Fe_3O_4 (point F), and of Fe^{II}_{aq} (point I) and FeOOH (point E), respectively. Reaction (3), which evolves very slowly, is represented by segment DE in buffered conditions. A path [AC'F'] corresponds to the formation of a mixture of goethite and magnetite when the oxygen concentration is lower; in such a case there are regions with goethite that forms where oxygen is immediately accessible and other less accessible regions where oxygen is lacking leading to Fe_3O_4 formation. For all dissolution-precipitation reactions, the carbonate species of the initial $GR(CO_3^{2-})$ are released into solution as well as Fe^{II} cations.

4.2.2. In situ *oxidation within the solid*

The rapid reaction of $GR(CO_3^{2-})$ with dissolved O_2 is described according to:

$$Fe^{II}_4\,Fe^{III}_2\,(OH)_{12}\,CO_3 + O_2 \Leftrightarrow Fe^{III}_6\,O_{12}\,H_8\,CO_3 + 2\,H_2O \qquad (5)$$

Note that $Fe^{III}_6\,O_{12}\,H_8\,CO_3$ is equivalent to $Fe^{III}_6\,O_4\,(OH)_8\,CO_3$ meaning that four hydroxyl ions out of twelve get deprotonated during the completion of the *in situ* oxidation. Reaction (5) corresponds to the line that links point B to point G (Fig. 6b). A continuous solid phase exists in between points B and G that corresponds to $GR(x)^*$,$Fe^{II}_{6(1-x)}\,Fe^{III}_{6x}\,O_{12}\,H_{2(7-3x)}\,CO_3$ compound, with variable composition x situated between 1/3 and 1. During the solid-state transformation $GR(CO_3^{2-}) \Rightarrow GR(CO_3^{2-})^*$, the kinetics is sufficiently rapid to inhibit any release of carbonate species into solution in contrast to the dissolution-precipitation mechanism; here, all Fe^{II} ions get oxidized into Fe^{III} rapidly within the solid state oxyhydroxycarbonate; only protons move.

As recalled in the introduction, the experimental observations concerning the solid state phases were carefully presented in other papers (Génin and Ruby, 2004, 2008; Génin et al., 2005; 2006c). They led us to present the compound with a variable composition by adding or subtracting protons at the apices of the octahedral sites where lie the Fe cations (Génin et al.,

2006c). The formula depends on the ratio x = {[Fe^{III}]/[Fe_{total}]}; thus we call it GR(x)* meaning formula $Fe^{II}_{6(1-x)}$ Fe^{III}_{6x} O_{12} $H_{2(7-3x)}$ CO_3. The ratio x balances the charges and the overall composition is well defined. However, it is not a solid solution where A atoms are substituted by B atoms and the question whether it is or not an ideal solution becomes irrelevant. The very notion of mixing entropy does not exist here from a statistical point of view and there exists *sensu stricto* no atomic diffusion.

In contrast, the usual notion of poles relates now to the ordered domains as determined from the magnetic behavior which was revealed by the Mössbauer spectra (Rusch et al., 2008). We have a mixture of magnetic hexagonal domains that correspond to various ordering of Fe^{III} cations: there exist three types of order corresponding to x = 0.33, 0.67 and 1, i.e. GR(x=0.33) where each Fe^{III} is surrounded by six Fe^{II}, GR*(x=0.67) where each Fe^{II} is surrounded by six Fe^{III} and ferric GR*(x=1). For each domain, the repulsion between Fe^{III} cations must be minimized. For any intermediate value of x, the mixture of domains may adjust their size to reach the exact composition x according to lever rule; for instance, if $x \in$ [0.33-0.67], the two poles are GR(x = 0.33) and GR*(x = 0.67), i.e. Fe^{II}_4 Fe^{III}_2 $(OH)_{12}$ CO_3 and Fe^{II}_2 Fe^{III}_4 O_{12} H_{10} CO_3; therefore, one gets a mixture of (3x-1) $\times$ GR*(x = 0.67) and (2-3x) $\times$ GR(x = 0.33) domains. It is in very good agreement with the quasi-linear variation of standard chemical potential of GR(x)*, i.e. $\mu°$[GR(x)*] ≈ (-619 + 57x) kJ mole $^{-1}$ (Fig. 3b of Ruby et al., 2006a), which was computed from the recorded data of electrode potential.

All occurrences of the mineral that have been observed in natural conditions happen to have, up till now, x values in the [0.33-0.67] range; it is due to thermodynamics and competition with magnetite in the range [0.67-1]. Thus, fougerite should be made similarly of such a mixture of magnetic domains within the same Fe^{II-III} oxyhydroxycarbonate crystal. It is also clear that the mineral may present a limited substitution of Fe cations by divalent or trivalent ions such as Mg^{2+} or Al^{3+}. In the laboratory, such substitutions are easily done (Aïssa

et al., 2004). However, we have not yet tested their influence on the mechanism of *in situ* protonation or deprotonation. Finally, there exists a remarkable agreement between XRD data reported in Table 2 where the d_{003} interplanar distances are 7.632, 7.569 and 7.565 Å for x = 0.33, 0.50 and 0.67 within GR(x)*, respectively, and the values reported by Christiansen et al. (2009) from patterns of samples found in ground water at Bornholm and Äspo (7.594 and 7.605 Å).

4.3. Reduction of ferric oxyhydroxides and formation of fougerite

As pointed out, the possibility to reduce ferric oxyhydroxides, i.e. common rusts, by dissimilatory iron-reducing bacteria in anaerobic conditions was a key point for identifying fougerite as being green rust. Thus, it is important to look for the path, which is followed during the bacterial reduction, in the Fe^{II}-Fe^{III} mass balance diagram (Fig. 7b). The initial conditions are represented by point E whatever the type of ferric hydroxide. In the absence of oxygen, bacteria reduce for respiration Fe^{III} ions and produce Fe^{II} ions that are dissolved within the solution. This is represented by a running point on tie-line EI. When reaching M, since this point in on tie-line FG, a reaction may form magnetite and ferric GR according to:

$$Fe^{II} + 8\,Fe^{III}OOH + CO_3^{2-} \Leftrightarrow Fe^{III}_6\,O_{12}\,H_8\,CO_3 + Fe^{II}\,Fe^{III}_2\,O_4 \qquad (6)$$

Formation of magnetite by bacterial activity was reported before that of GR(CO_3^{2-}) (Fredrickson et al., 1998; Ona-Nguema et al., 2002). In contrast, if the bacterial reduction is fast enough, point M is overshot and point N is reached leading to $Fe^{II}\,Fe^{III}_5\,O_{12}\,H_9\,CO_3$. One unique compound forms now by protonation on line NB; it is $Fe^{II\text{-}III}$ oxyhydroxycarbonate GR(x)*, $Fe^{II}_{6(1-x)}\,Fe^{III}_{6x}\,O_{12}\,H_{2(7-3x)}\,CO_3$, for a value of $x \in [1/3, 5/6]$. The corresponding reaction is now:

$$Fe^{II}_{6[1-(x+dx)]}\,Fe^{III}_{6(x+dx)}\,O_{12}\,H_{2[7-3(x+dx)]}\,CO_3 + 6dx\,H^+ + 6dx\,e^- \Leftrightarrow Fe^{II}_{6(1-x)}\,Fe^{III}_{6x}\,O_{12}\,H_{2(7-3x)}\,CO_3,$$

This can be written symbolically as:

$$GR(x+dx)^* + dx\ H^+ + dx\ e^- \Leftrightarrow GR(x)^* \quad (7)$$

Values of standard chemical potential $\mu^0[GR(x)^*]$ were determined for $GR(x)^*$ at various values x of the ferric molar fraction, i.e. -600.27, -596.56 and -592.29 kJ mole^{-1} for x = 0.33, 0.41 and 0.50, respectively (Ruby et al., 2006a); these allowed us to plot E_h-pH Pourbaix diagrams (Fig. 7a) for the *in situ* continuous reduction by protonation along reaction (7). A set of parallel lines displays Nernst's law with slope (- 0.0591). This illustrates equilibrium conditions of reaction (7) during reduction within $Fe^{II}_{6(1-x)}\,Fe^{III}_{6x}\,O_{12}\,H_{2(7-3x)}\,CO_3$ compound.

4.4. Thermodynamic properties of Fe^{II-III} oxyhydroxycarbonate and field experiments

These values of $\mu^0[GR(x)^*]$ allow us to plot E_h-pH Pourbaix diagrams corresponding to the oxidation of a given $GR(x)^*$ via the dissolution-precipitation mechanism as usually observed in natural conditions (Fig. 8 & 9). Because of the field observations made from the upper part of hydromorphic soils in Fougères (Abdelmoula et al., 1998), γ-FeOOH lepidocrocite was chosen as ferric oxyhydroxide in equilibrium with fougerite (Fig. 8). Most stable ferric oxyhydroxide, i.e. α-FeOOH goethite, was also considered (Fig. 9). Mean values of E_h and pH that were measured in the field during the period from February 1999 to June 2000 (Féder et al., 2005) are also reported by black dots for comparison (Fig. 8 & 9). For both diagrams involving either lepidocrocite or goethite, the size of the stability domain of $GR(x)^*$ decreases when x increases and $GR^*(x = 0.5)$ is completely metastable with respect to α-FeOOH goethite (Fig. 9c). Almost all E_h-pH data measured *in situ* in the field are situated inside the stability domain of $GR(x)^*$ when lepidocrocite is considered as the final product of oxidation (Fig. 8a & b). Moreover, most field data are close to the line corresponding to the equilibrium between $GR(x)^*$ and Fe^{2+}_{aq} for an activity $a(Fe^{2+})$ situated between ~10^{-2} and 10^{-4}; this last

value is close to the mean value of Fe^{2+} concentration measured in the soil aqueous medium by Féder et al. (2005). As pointed out in previous studies (Trolard et al., 1997, Génin et al., 1998b) only equilibrium between GR and Fe^{2+} may explain the relatively high concentrations of Fe^{2+} present in soil solution because the reductive dissolution of Fe^{III} oxyhydroxides is less favourable. This favours the fact that equilibrium between Fe^{II-III} oxyhydroxycarbonate GR(*x*)* and Fe^{2+} would control the quantity of ferrous species measured in soil solution. Another question arises about the eventual presence in an unsaturated zone of soil of the fully oxidized ferric form GR(CO_3^{2-})* by contact with atmosphere. Careful examination of ferric oxyhydroxides formed in fougerite vicinity may provide such information.

5. CONCLUSIONS

Oxidation of synthetic carbonate green rust GR(CO_3^{2-}) where $x = 1/3$ can occur either by dissolution and precipitation of a ferric $Fe^{III}OOH$ oxyhydroxide or by continuous *in situ* deprotonation through the Fe^{II-III} oxyhydroxycarbonate GR(*x*)* of general formula $Fe^{II}_{6(1-x)}\ Fe^{III}_{6x}\ O_{12}\ H_{2(7-3x)}\ CO_3 \bullet 3H_2O$, where the ferric molar ratio *x* is limited to the]0.33-0.67] range. Its structure strongly resembles that of the Fe^{II-III} hydroxycarbonate GR(CO_3^{2-}), $Fe^{II}_4\ Fe^{III}_2\ (OH)_{12}\ CO_3 \bullet 3H_2O$, which belongs to the layered double hydroxide family; it can be prepared in the laboratory by fast oxidation of GR(CO_3^{2-}), through an *in situ* deprotonation of some OH^- ions without destroying the hexagonal GR crystals and by keeping CO_3^{2-} anions in interlayers at their position. Various routes for oxidizing GR(CO_3^{2-}) were described within the frame of the mass-balance diagram, i.e. dissolution-precipitation of FeOOH versus *in situ* deprotonation. Bacterial reduction of ferric oxyhydroxide may be followed satisfactorily within the same frame and corresponds to the actual formation of the fougerite mineral in the water table. Thermodynamic data on the synthetic compound allows

us to rationalise Fe^{2+} ion concentrations found in groundwater as collected from the literature and E_h-pH diagrams of GR(*x*)* when *x* varies have been drawn. The identification of the mineral that contains Fe in gleysols and is responsible for its bluish-green colour seems now to be fully accomplished.

ACKNOWLEDGMENTS

We thank Région-Lorraine and Université Henri Poincaré for a postdocdoral grant (V. Khare). We thank Dr Y.Wang (IMPMC- Université P. et M. Curie) and G. Medjahdi (LCSM-Nancy-Université) for XRD experiments. We thank Jean-Paul Moulin (LCPME- Nancy-Université) for designing the MIMOS cell. The authors would like to thank the reviewers for very valuable suggestions that improved the text considerably.

REFERENCES

Abdelmoula M., Refait Ph., Drissi S. H., Mihé J. P. and Génin J.-M. R. (1996) Conversion electron Mössbauer spectroscopy and X-ray diffraction studies of the formation of carbonate-containing green rust one by corrosion of metallic iron in $NaHCO_3$ and ($NaHCO_3$ + NaCl) solutions. *Corros. Sci*. **38**, 623-633.

Abdelmoula M., Trolard F., Bourrié G. and Génin J.-M. R. (1998) Evidence for the Fe(II)-Fe(III) green rust " fougerite " mineral occurrence in a hydromorphic soil and its transformation with depth. *Hyperfine Interact.* **112**, 235–238.

Aïssa R., Ruby C., Géhin, A., Abdelmoula M. and Génin J.-M. R. (2004) Synthesis by coprecipitation of Al-substituted hydroxysulphate green rust $Fe^{II}_4\ Fe^{III}_{(2-y)}\ Al^{III}_y\ (OH)_{12}\ SO_4\ .\ nH_2O$. *Hyperfine Interact.* **156/157**, 445-451.

Aïssa R., François M., Ruby C., Fauth F., Medjahdi G., Abdelmoula M. and Génin J.-M. R. (2006) Formation and crystallographic structure of hydroxysulphate and hydroxycarbonate green rusts synthesized by coprecipitation. *J. Phys. Chem. Solids* **67**, 1016-1019.

Benali O., Abdelmoula M., Refait Ph. and Génin J.-M. R. (2001) Effect of orthophosphate on the oxidation products of Fe(II)-Fe(III) hydroxycarbonate: the transformation of green rust to ferrihydrite. *Geochim. Cosmochim. Acta* **65**, 1715-1726.

Bernal J. D., Dasgupta D. and Mackay A. L. (1959) The oxides and hydroxides of iron and their structural inter-relationships. *Clay Min. Bull.* **4,** 15-30.

Bocher F., Géhin A., Ruby C., Ghanbaja J., Abdelmoula M. and Génin J.-M. R. (2004) Coprecipitation of Fe (II-III) hydroxycarbonate green rust stabilised by phosphate adsorption. *Solid State Sci.* **6**, 117-124.

Christiansen B. C., Balic-Zunic T., Dideriksen K. and Stipp S. L. S. (2009) Identification of green rust in groundwater. *Environ. Sci. Technol.* **43**, 3436-3441.

Drissi H., Refait Ph. and Génin J.-M. R. (1994) The oxidation of $Fe(OH)_2$ in the presence of carbonate ions : structure of carbonated green rust one. *Hyperfine Interact.* 90, 395-400.

Drissi S. H., Refait Ph., Abdelmoula M. and Génin J.-M. R. (1995) Preparation and thermodynamic properties of Fe(II)-Fe(III) hydroxycarbonate (green rust one); Pourbaix diagram of iron in carbonate-containing aqueous media. *Corros. Sci.* **37**, 2025-2041.

Ernstsen V. and Mørup S. (1992) Nitrate reduction in clayey till by Fe(II) in clay minerals. *Hyperfine Interact.* **70**, 1001-1004.

Ernstsen V. (1996) Reduction of nitrate by Fe^{2+} in clay minerals. *Clay Clay Min.* **44**, 599-608.

Féder F., Trolard F., Klingelhöfer G. and Bourrié G. (2005) In situ Mössbauer spectroscopy: Evidence for green rust (fougerite) in a gleysol and its mineralogical transformations with time and depth. *Geochim. Cosmochim. Acta* **69**, 4463-4483.

Feitknecht W. and Keller G. (1950) Uber die Dunkelgrünen Hydroxyverbindungen des Eisens. *Z. Anorg. Allg. Chem.* **262,** 61-68.

Fredrickson J. K., Zachara J. M., Kennedy D. W., Dong H., Onstott T. C., Hinman N. H. and Li S. (1998) Biogenic iron mineralization accompanying the dissimilatory reduction of hydrous ferric oxide by a groundwater bacterium. *Geochim. Cosmochim. Acta* **62**, 3239-3257.

Génin J.-M. R. and Ruby C. (2004) Anion and cation distribution in Fe(II-III) hydroxysalts green rusts from XRD and Mössbauer analysis (carbonate, chloride, sulphate…); the "fougerite" mineral. *Solid State Sci.* **6**, 705-718.

Génin J.-M. R. and Ruby C. (2008) Composition and anion ordering in some Fe^{II-III} hydroxysalt green rusts (carbonate, oxalate, methanoate); the fougerite mineral. *Solid State Sci.* **10**, 244-259

Génin J.-M. R., Bauer Ph., Olowe A. and Rézel D. (1986) Mössbauer study of the kinetics of simulated corrosion process of iron in chlorinated aqueous solution around room temperature: the hyperfine structure of ferrous hydroxides and green rust 1. *Hyperfine Interact* .**29**, 1355-58.

Génin J.-M. R., Olowe A.A , Refait Ph. and Simon L. (1996) On the stoichiometry and Pourbaix diagram of Fe(II)-Fe(III) hydroxy-sulphate or sulphate-containing green rust 2 ; an electrochemical and Mössbauer spectroscopy study. *Corros. Sci.* **38**, 1751-1762.

Génin J.-M. R., Refait Ph., Simon L. and Drissi S. H. (1998a) Preparation and E_h-pH diagrams of Fe(II)-Fe(III) green rust compounds; hyperfine interaction characteristics and stoichiometry of hydroxy-chloride, -sulphate and -carbonate. *Hyperfine Interact.* **111**, 313-318.

Génin J.-M. R., Bourrié G., Trolard F., Abdelmoula M., Jaffrezic A., Refait Ph., Maître V., Humbert B. and Herbillon A. (1998b) Thermodynamic equilibria in aqueous suspensions of synthetic and natural iron(II)-iron(III) green rusts: occurrences of the mineral in hydromorphic soils. *Environ. Sci. Technol.* **32**, 1058-1068.

Génin J.-M. R., Aïssa R., Géhin A., Abdelmoula M., Benali O., Ernstsen V., Ona-Nguema G., Upadhyay C. and Ruby C. (2005) Fougerite and Fe^{II-III} hydroxycarbonate green rust: ordering, deprotonation and/or cation substitution; structure of hydrotalcite-like compounds and mythic hydroxide $Fe(OH)_{(2+x)}$. *Solid State Sci.* **7**, 545-572.

Génin J.-M. R., Abdelmoula M., Ruby C., and Upadhyay C. (2006a) Speciation of iron; characterisation and structure of green rusts and Fe^{II-III} oxyhydroycarbonate fougerite. *C.-R. Geoscience* **338**, 402-419.

Génin J.-M. R., Ruby C., Géhin A. and Refait Ph. (2006b) Synthesis of green rust by oxidation of $Fe(OH)_2$, their products of oxidation and reduction of ferric oxyhydroxides; E_h-pH Pourbaix diagrams. *C.-R. Geoscience* **338**, 433-446.

Génin J.-M. R., Ruby C. and Upadhyay C. (2006c) Structure and thermodynamics of ferrous, stoichiometric and ferric oxyhydroxycarbonate green rusts; redox flexibility and fougerite mineral. *Solid State Sci.* **8**, 1330–1343.

Girard A. and Chaudron G. (1935) Sur la constitution de la rouille. *C.-R. Acad. Sci. Paris* **200**, 127-129.

Hansen H. C. B. (1989) Composition, stabilization, and light absorption of Fe(II)Fe(III) hydroxy-carbonate ("green rust"). *Clay Miner.* **24**, 663-669.

Hansen H. C. B (2001) in *Layered double hydroxides: present and future: Environmental Chemistry of Iron(II)-Iron(III) LDHs (Green rusts),* Nova Science publishers, 469-493.

Klingelhöfer G., Fegley Jr B., Morris R. V., Kankeleit E., Held P., Elvanov E. and Priloutskii O. (1996) Mineralogical analysis of Martian soil and rock by a miniaturized backscattering Mössbauer spectrometer. *Planet Space Sci.* **44**, 1277-1288.

Legrand L., Abdelmoula M., Géhin A., Chaussé A. and Génin J.-M. R. (2001) Electrochemical formation of a new Fe(II)-Fe(III) hydroxycarbonate green rust: characterisation and morphology. *Electrochim. Acta* **46**, 1815-1822.

Legrand L., Mazerolles L. and Chaussé A. (2004) The oxidation of carbonate green rust into ferric phases: solid-state reaction or transformation via solution. *Geochim. Cosmochim. Acta* **68**, 3497-3507.

Mullet M., Guillemin Y. and Ruby C. (2008) Oxidation and deprotonation of synthetic Fe^{II}-Fe^{III} (oxy)hydroxycarbonate green rust: An X-ray photoelectron study. *J. Solid State Chem.* **181**, 81-89.

Murad E. and Taylor R. M. (1984) The Mössbauer spectra of hydroxycarbonate green rusts. *Clay Minerals* **19**, 77-83.

Olowe A., Génin J.-M. R. and Bauer Ph. (1987) Hyperfine interactions and structures of ferrous hydroxide and green rust 2 in sulfated aqueous media. *Hyperfine Interact.* **41**, 501-504.

Ona-Nguema G., Abdelmoula M., Jorand F., Benali O., Géhin A., Block J.-C. and Génin J.-M. R. (2002) Iron (II,III) hydroxycarbonate green rust formation and stabilization from lepidocrocite bioreduction. *Environ. Sci. Technol.* **36**, 16-20.

Refait Ph. and Génin J.-M. R. (1993) The oxidation of ferrous hydroxide in chloride-containing aqueous media and Pourbaix diagrams of green rust one. *Corros. Sci.* **34**, 797-819.

Refait Ph., Abdelmoula M., Trolard F., Génin J.-M. R., Ehrhardt J.-J. and Bourrié G. (2001) Mössbauer and XAS study of a green rust mineral; the partial substitution of Fe^{2+} by Mg^{2+}. *Amer. Miner.* **86**, 731-739.

Refait Ph., Benali O., Abdelmoula M. and Génin J.-M. R. (2003) Formation of 'ferric green rust' and/or ferrihydrite by fast oxidation of iron(II–III) hydroxychloride green rust. *Corros. Sci.* **45**, 2435-2449.

Refait Ph., Reffass M., Landoulsi J., Sabot R. and Jeannin M. (2007) Role of phosphate species during the formation and transformation of the Fe(II–III) hydroxycarbonate green rust. *Colloid Surface A* **299,** 29-37.

Rodionov D., Klingelhöfer G., Bernhardt B., Schröder C., Blumers M., Kane S., Trolard F., Bourrié G. and Génin J.-M. R. (2006) Automated Mössbauer spectroscopy in the field and monitoring of fougerite. *Hyperfine Interact.* **167**, 869-873.

Ruby C., Upadhyay C., Géhin A., Ona-Nguema G. and Génin J.-M. R. (2006a) In situ redox flexibility of Fe^{II-III} oxyhydroxycarbonate green rust and fougerite. *Environ. Sci. Technol.* **40**, 4696-4702.

Ruby C., Aïssa R., Géhin A., Cortot J., Abdelmoula M. and Génin J.-M. R. (2006b) Green rusts synthesis by coprecipitation of Fe^{II}–Fe^{III} ions and mass-balance diagram. *C. R. Geoscience* **338,** 420-432.

Ruby C., Géhin A., Aïssa R. and Génin J.-M. R. (2006c) Mass-balance diagram and E_h-pH diagram of Fe^{II-III} oxyhydroxycarbonate green rusts; redox flexibility and fougerite mineral. *Corros. Sci.* **48**, 3824-3837.

Rusch B., Génin J.-M. R., Ruby C., Abdelmoula M. and Bonville P. (2008) Ferrimagnetic properties of Fe(II-III) (oxy-)hydroxycarbonate green rust. *Solid State Sci.* **10**, 40-49.

Taylor R. M. (1980) Formation and properties of Fe(II)-Fe(III) hydroxycarbonate and its possible significance in soil formation. *Clay Miner.* **15,** 369-382.

Taylor R. M. (1982) Color in soils and sediments - A review. *Development in Sedimentology*, 749-761.

Trolard F., Génin J.-M. R., Abdelmoula M., Bourrié G., Humbert B. and Herbillon A. (1997) Identification of a green rust mineral in a reductomorphic soil by Mössbauer and Raman spectroscopy. *Geochim. Cosmochim. Acta* **61**, 1107-1111.

Vandenberghe R. E., Barrero C. A., Da Costa G. M., Van San E. and De Grave E. (2000) Mössbauer characterization of iron oxides and (oxy)hydroxides: the present state of the art**.** *Hyperfine Interact.* **126**, 247-259.

Vysostskii G. N. (1905) Gley, *Pochvovedeniye (Eurasian Soil Sci.)* **4,** 291-327.

Table 1

Experimental conditions and nature of the final oxidation products; $X(O_2)$ % is the percentage of oxygen present in the gas flow. The oxidation velocity is determined by using the oxidation time t_f at the equivalent point of Fig. 3a. The efficiency of the oxidation is determined by the ratio $V(O_2)$ / $F(O_2)$ where $F(O_2)$ is the flow of O_2 bubbled into the solution. Experiments are carried out at pH 9.

Type of oxidation	Controlled O_2 bubbling	Controlled O_2 bubbling	Controlled O_2 bubbling	Controlled O_2 bubbling	Air oxidation
$X(O_2)$ (%)	2.7	6.7	13.3	20	-
magnetic stirring (rpm)	375	375	375	375	750
oxidation time t_f (min)	700	440	290	170	80
$V(O_2)$ Oxidation velocity (Mole per day)	0.005	0.011	0.016	0.028	0.06
$F(O_2)$ Flow of O_2 (Mole per day)	0.4	1	1.9	2.9	-
Efficiency $V(O_2)$ / $F(O_2)$ (%)	1.2	1.1	0.9	1	-
Colour of the final product	Black	Yellow-Brown	Yellow-Brown	Yellow-Brown	Orange-Brown
Oxidation products	Magnetite + Goethite	Goethite	Goethite	Goethite	GR*

Table 2

Distances and cell parameters computed from the XRD data presented in Fig. 1.

Ferric molar fraction / d_{hkl} distances and cell parameters	x = 0.33	x = 0.5	x = 0.67	x = 0.83	x = 1
d_{003} (Å)	7.632	7.569	7.565	7.54	~ 7.34
d_{012} (Å)	2.679	2.669	2.672	-	-
c (Å)	22.896	22.707	22.695	-	-
a (Å)	3.182	3.169	3.173	-	-

Table 3

Mössbauer hyperfine parameters of the spectra presented in figure 2. The spectra were fitted with either Lorentzian shape lines (Fig. 2α) or a Voigt profile analysis [Fig. (2β-ε) : *CS* : center shift with respect to metallic α-Fe at room temperature (Lorentzian shape lines); <*CS*> : center shift at the maximum of the Gaussian distribution (Voigt profiles), Δ : quadrupole splitting, <Δ> : quadrupole splitting at the maximum of the Gaussian distribution, *RA* : relative area; *x* : ferric molar fraction {[Fe^{III}] / [Fe_{total}]} either measured by Mössbauer spectroscopy or targeted from the added quantity of H_2O_2.

Fig. 2	Component	*CS* or <*CS*> (mm s^{-1})	Δ or <Δ> (mm s^{-1})	*RA* (%)	*x* (measured)	*x* (targeted)
α	D_1 (Fe^{II})	1.13	2.51	54		
	D_2 (Fe^{II})	0.90	1.91	11		
	D_3 (Fe^{III})	0.40	0.40	35	0.35	0.33
β	D_1 (Fe^{II})	1.25	2.39	26		
	D_2 (Fe^{II})	1.04	2.26	18		
	D_3 (Fe^{III})	0.41	0.31	26		
	D_4 (Fe^{III})	0.29	1.03	28	0.54	0.5
γ	D_1 (Fe^{II})	1.20	2.42	28		
	D_2 (Fe^{II})	1.16	1.65	9		
	D_3 (Fe^{III})	0.36	0.39	22		
	D_4 (Fe^{III})	0.29	0.96	41	0.63	0.67
δ	D_1 (Fe^{II})	1.21	1.97	15		
	D_3 (Fe^{III})	0.35	0.43	28		
	D_4 (Fe^{III})	0.35	0.90	57	0.85	0.83
ε	D (Fe^{III})	0.45	0.98	100	1	1

Table 4

Mössbauer hyperfine parameters of the spectra presented in figure 5. *CS* : center shift with respect to metallic α-Fe at room temperature; Δ : quadrupole splitting in the paramagnetic state or ε : quadrupole shift ; *H* : Hyperfine magnetic field; *RA* : relative area. Spectrum of Fig. 5b was not computed due to relaxation behaviour.

Figure	Component	*CS* (mm s^{-1})	Δ or ε (mm s^{-1})	*H* (kOe)	*RA* (%)
5a	*D* (Fe^{III})	0.38	0.57	-	12
	S_1	0.34	0	500	14
	S_2	0.53	0	483	41
	S_3	0.47	0	446	33
5c	*D* (Fe^{III})	0.39	0.68	-	100

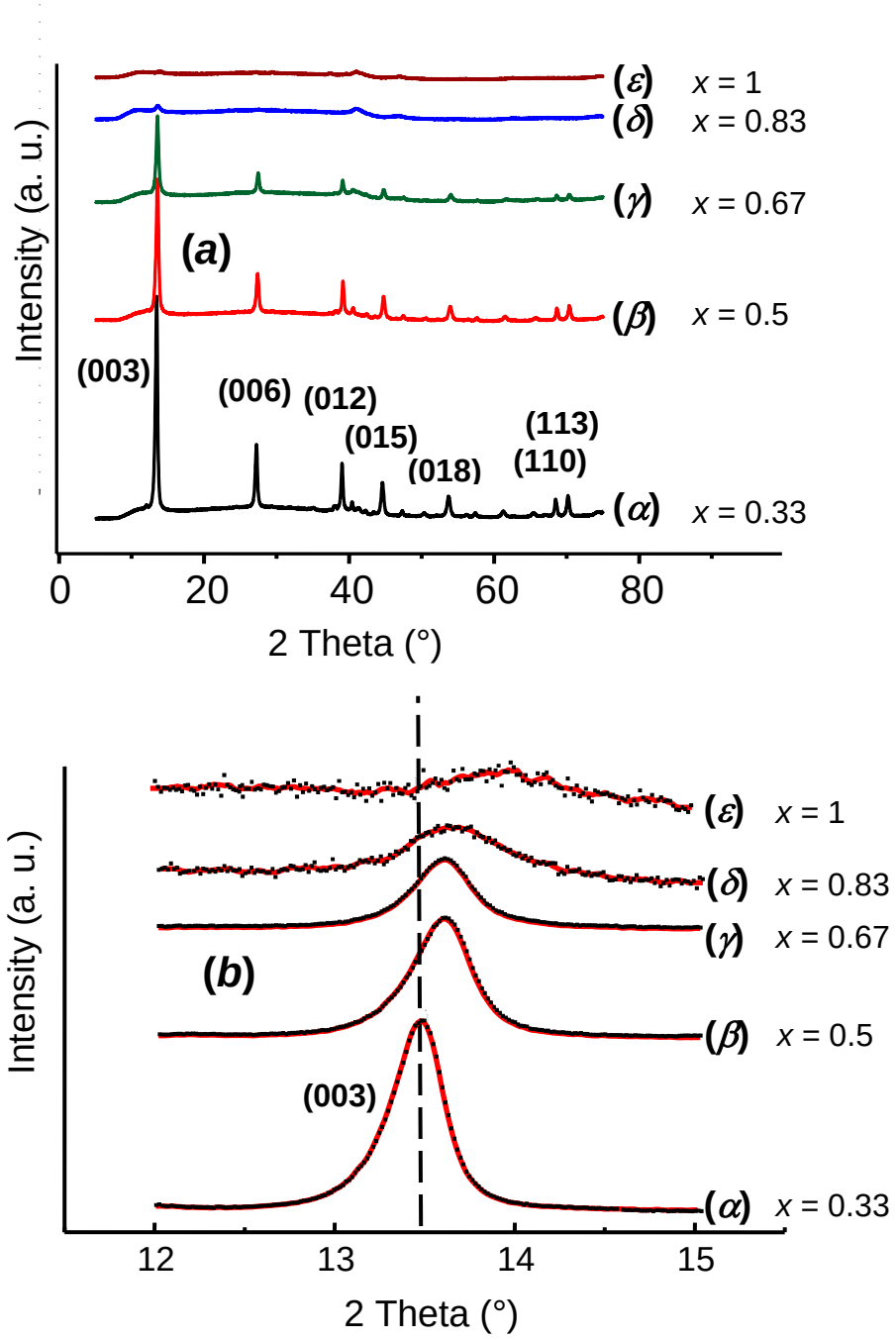

Figure.1. (a) X-ray diffractograms of GR(CO_3^{2-}) at x = 0.33 and GR(CO_3^{2-})* oxidised at different values of the ferric molar fraction x. [λ (CoK_α) = 0.17889 nm].

(b) Zoom of the (003) peak region.

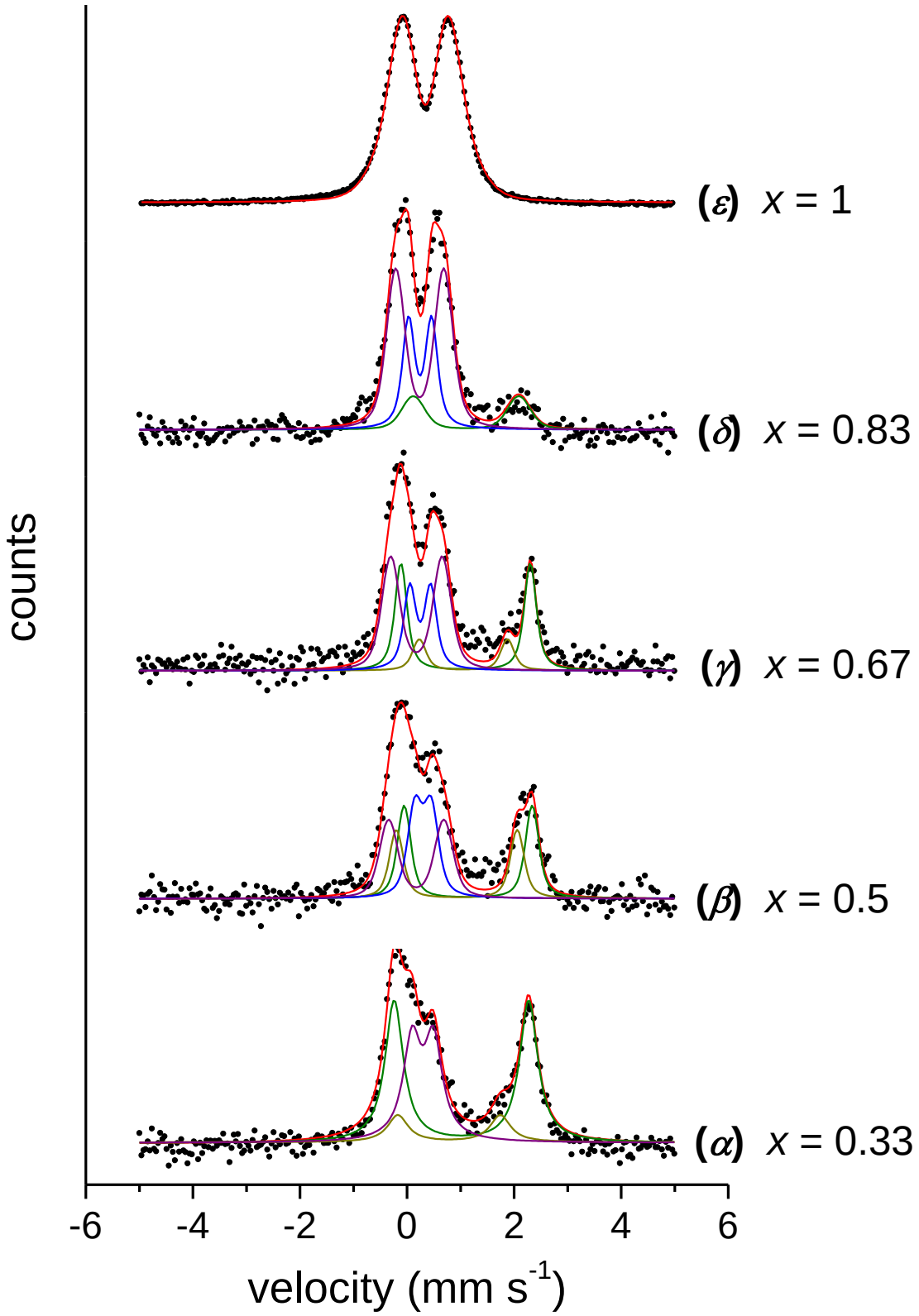

Figure.2. Backscattered Mössbauer spectra of GR(CO_3^{2-}) at x = 0.33 and GR(CO_3^{2-})* oxidised at different values of the ferric molar fraction x. The spectra are recorded with MIMOS at room temperature.

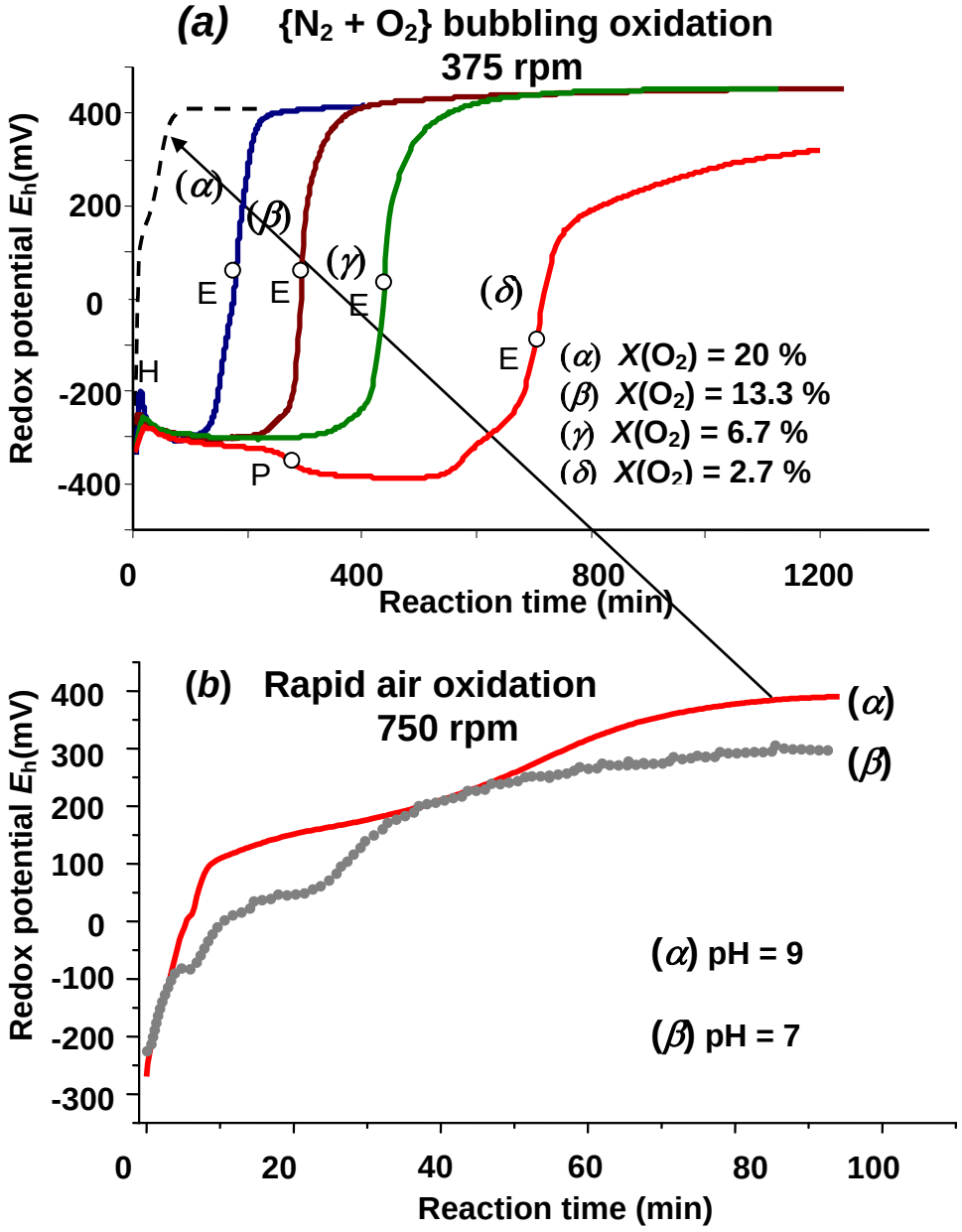

Fig. 3. Evolution of the redox potential E_h measured in the aqueous suspension during (*a*) controlled air bubbling oxidation (375 rpm) and
(*b*) rapid air oxidation (750 rpm). Dotted curve in (a) is curve (α) of (b).

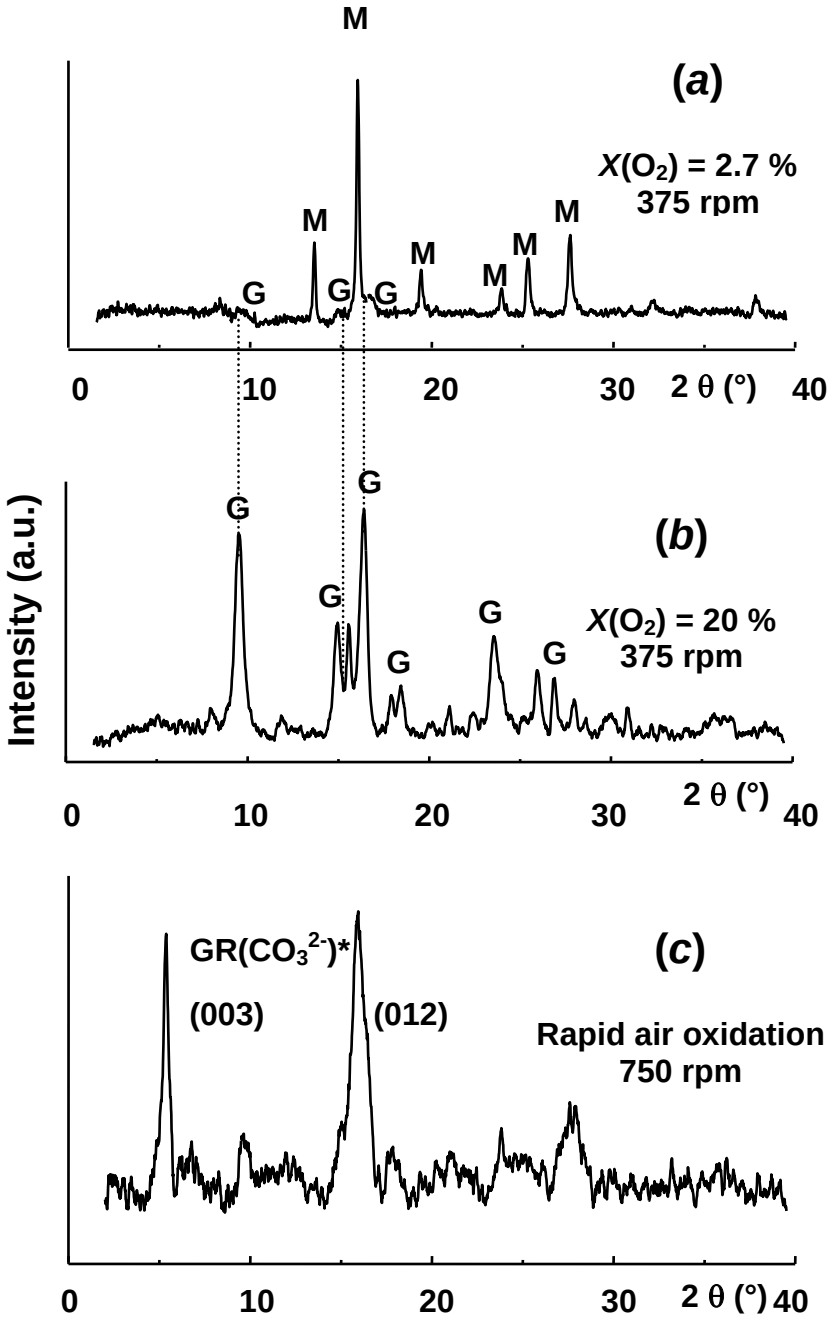

Fig. 4. X-ray diffractograms [λ (MoK_α) = 0.07093 nm] of the end products obtained after oxidation of $GR(CO_3^{2-})$.
(a) & (b) Synthetic air bubbling experiments at 375 rpm (G: goethite, M: magnetite),
(c) Rapid air oxidation at 750 rpm: ferric $GR(CO_3^{2-})$*

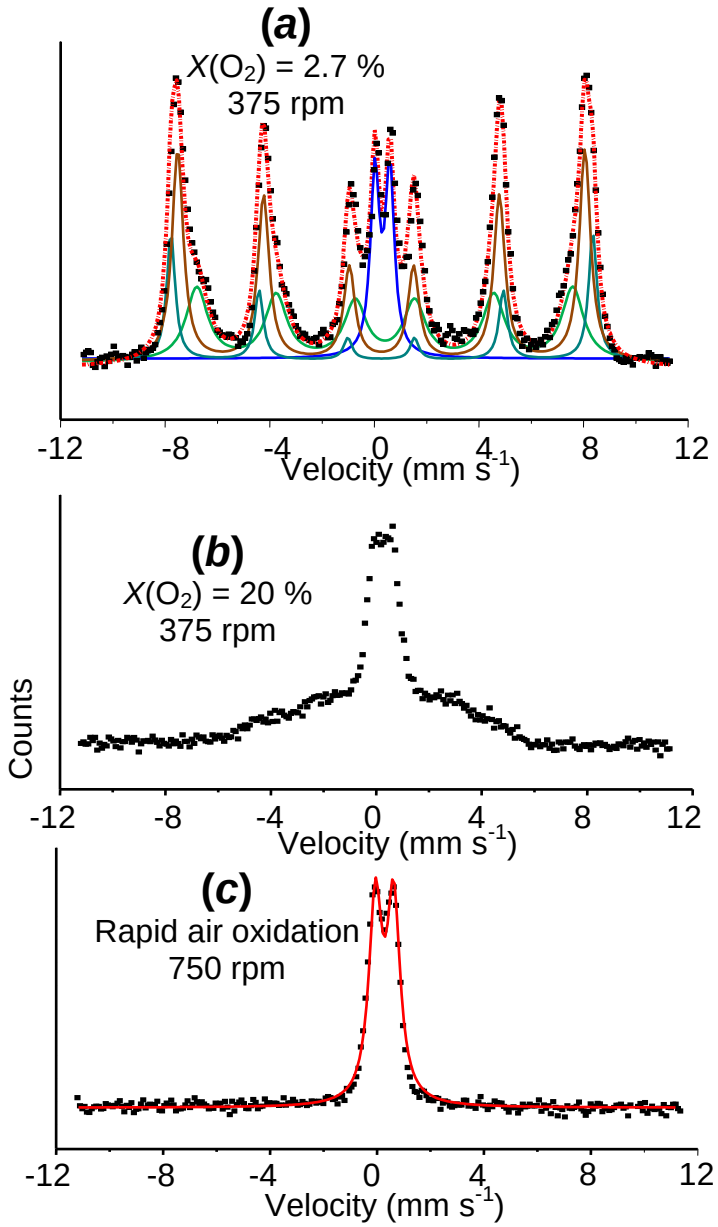

Fig.5. Mössbauer spectra recorded at room temperature of the end products obtained after the oxidation of GR(CO_3^{2-}): (a) & (b) Air bubbling experiments (375 rpm), (c) Rapid air oxidation (750 rpm).

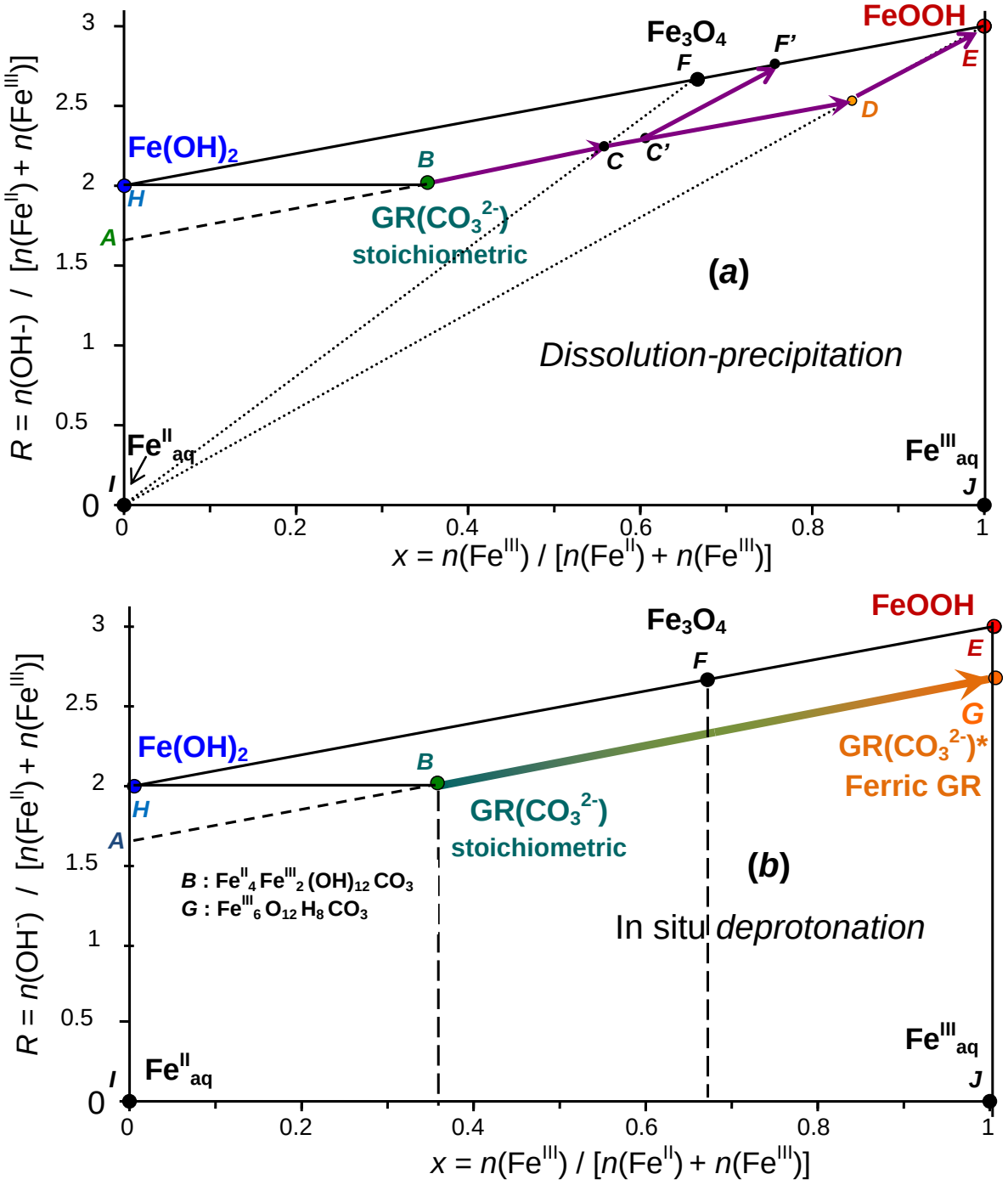

Fig. 6. Fe^{II}-Fe^{III} mass balance diagram showing various paths for the oxidation of Fe^{II-III} hydroxycarbonate $GR(CO_3^{2-})$ (a) forming ferric oxyhydroxide FeOOH by dissolution and precipitation mechanism and (b) forming ferric oxyhydroxycarbonate $GR(CO_3^{2-})$* by *in situ* deprotonation.

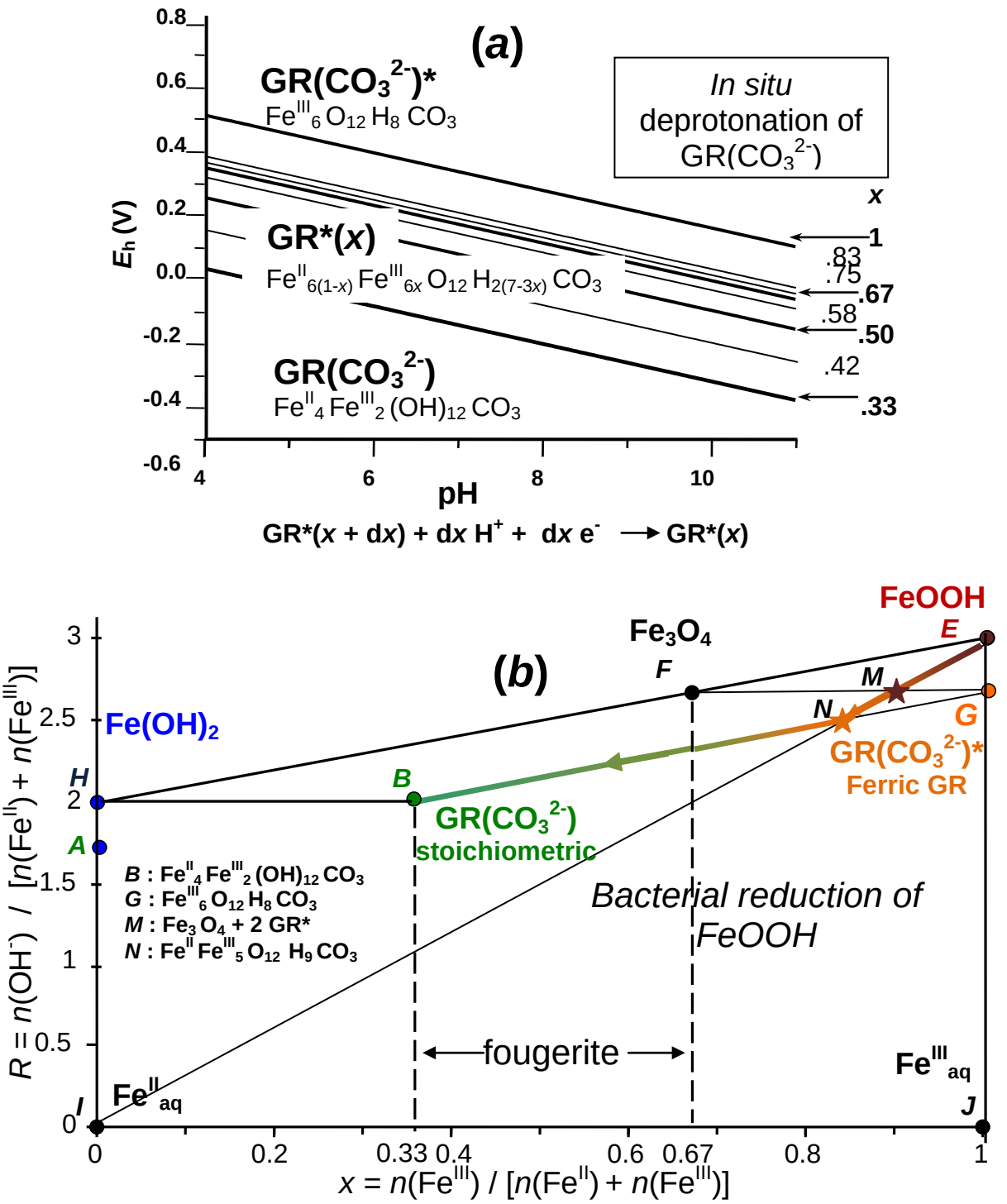

Fig.7. (a) E_h-pH Pourbaix diagram of the continuous reduction-oxidation by *in situ* protonation-deprotonation mechanism of oxyhydroxycarbonate GR*(*x*) (according to Ruby et al., 2006)
(b) Fe^{II}-Fe^{III} mass-balance diagram showing the path followed during the reduction of a oxyhydroxide FeOOH by dissimilatory iron-reducing bacteria in anoxic conditions: the formation of fougerite.

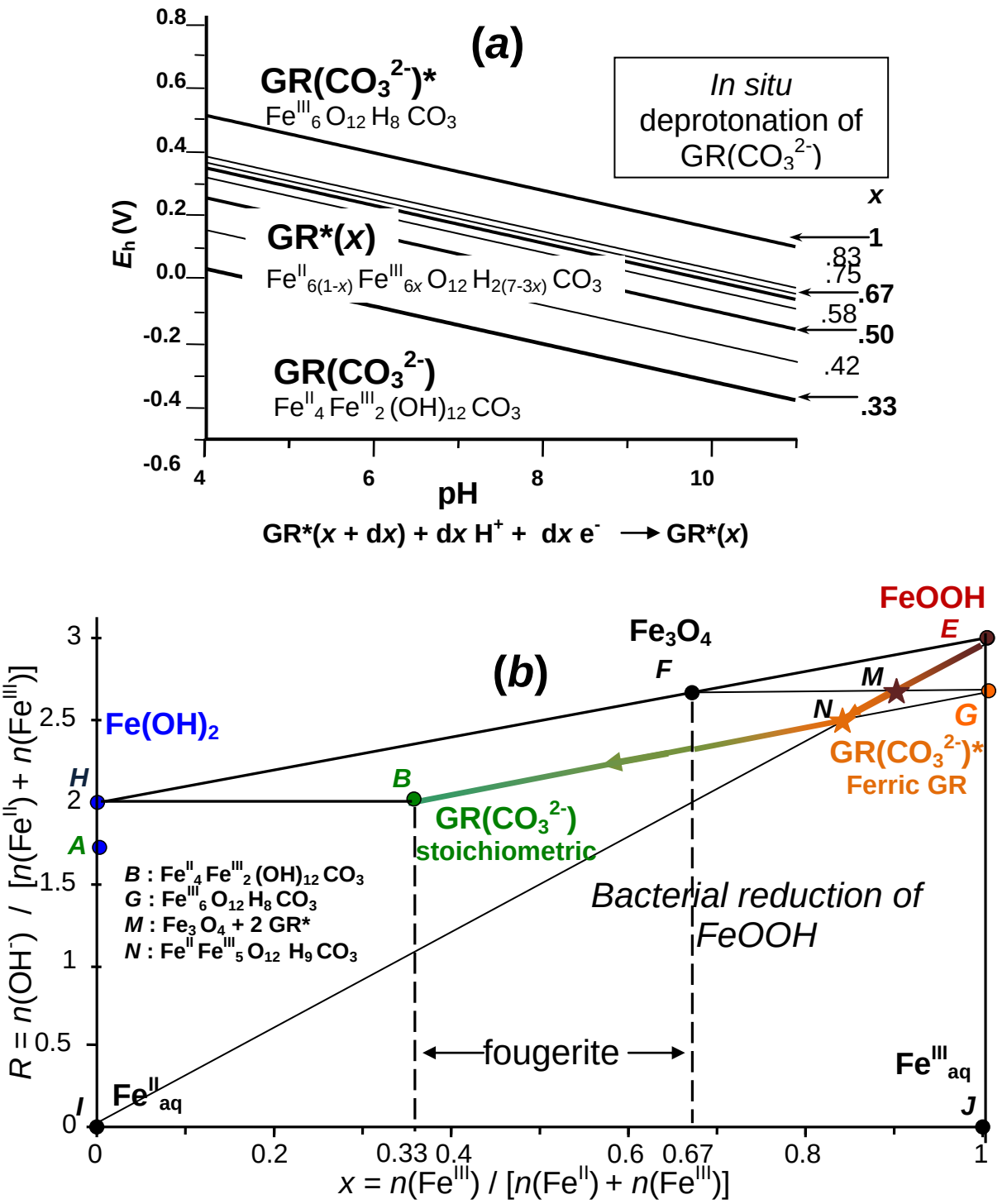

Fig.7. (a) E_h-pH Pourbaix diagram of the continuous reduction-oxidation by *in situ* protonation-deprotonation mechanism of oxyhydroxycarbonate GR*(*x*) (according to Ruby et al., 2006)
(b) Fe^{II}-Fe^{III} mass-balance diagram showing the path followed during the reduction of a oxyhydroxide FeOOH by dissimilatory iron-reducing bacteria in anoxic conditions: the formation of fougerite.

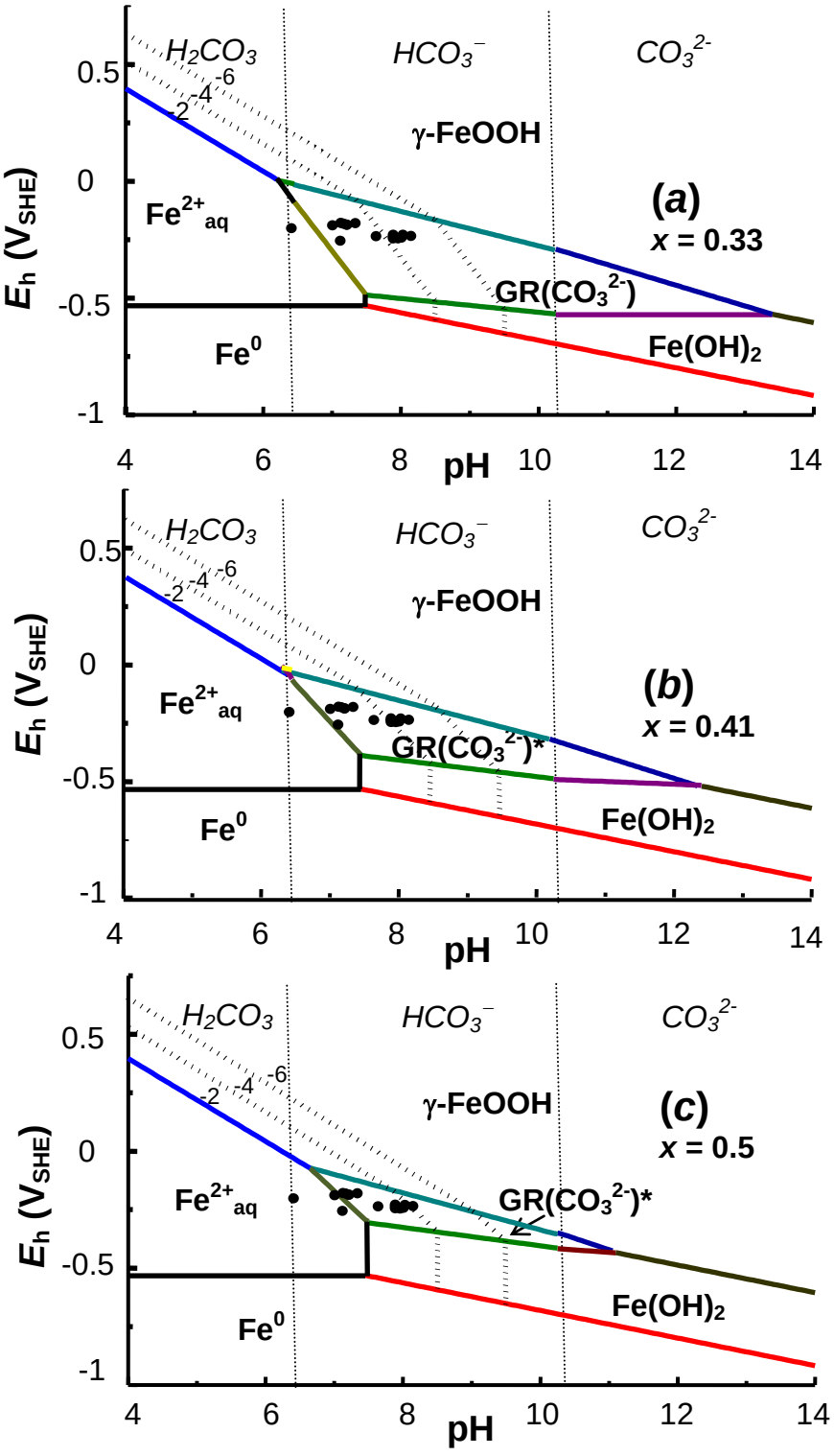

Fig. 8. E_h-pH Pourbaix diagrams of iron compounds in a carbonated aqueous medium. The activity of carbonate species is fixed at a value of 10^{-2}. The ferric oxyhydroxide is lepidocrocite γ-FeOOH. Field analyses are represented by dots (Féder et al., 2005).

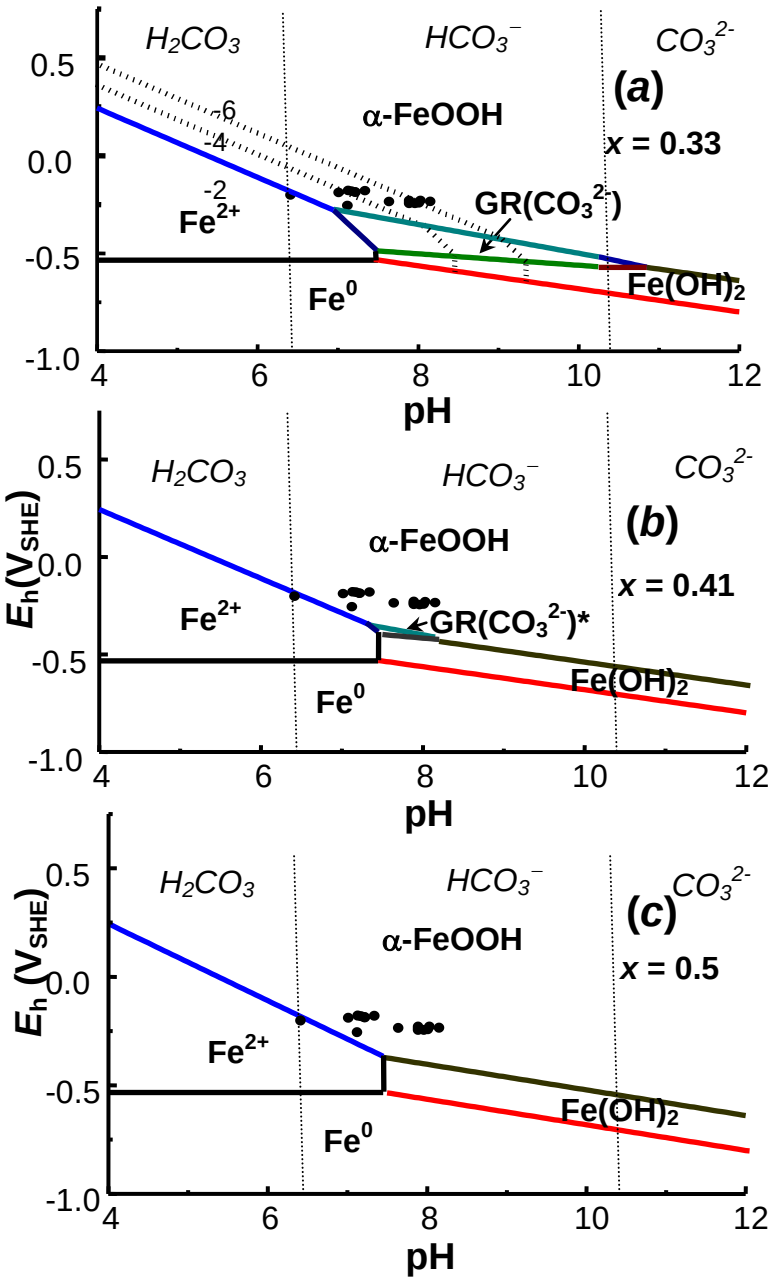

Fig. 9. E_h-pH Pourbaix diagrams of iron compounds in a carbonated aqueous medium. The activity of carbonate species is fixed at a value of 10^{-2}. The ferric oxyhydroxide is goethite α-FeOOH, the most stable one. Field analyses are represented by dots (Féder et al., 2005).